ResearchGate

See discussions, stats, and author profiles for this publication at: https://www.researchgate.net/publication/258805867

Polymer/TiO2Hybrid Nanoparticles with Highly Effective UV-Screening but Eliminated Photocatalytic Activity

ARTICLE *in* MACROMOLECULES · JANUARY 2013

Impact Factor: 5.8 · DOI: 10.1021/ma3022019

CITATIONS
25

READS
52

4 AUTHORS, INCLUDING:

Jianzhong Du
Tongji University
68 PUBLICATIONS **2,859** CITATIONS

SEE PROFILE

Available from: Jianzhong Du
Retrieved on: 28 January 2016

Macromolecules

Article

pubs.acs.org/Macromolecules

Polymer/TiO_2 Hybrid Nanoparticles with Highly Effective UV-Screening but Eliminated Photocatalytic Activity

Jie Xiao, Wenqin Chen, Fangyingkai Wang, and Jianzhong Du*

School of Materials Science and Engineering, Tongji University, 4800 Caoan Road, Shanghai 201804, China

Supporting Information

ABSTRACT: TiO_2 nanoparticle has been considered as a safe sunscreen agent to reduce the skin cancer risk when exposed to sunlight. However, recently it was found that TiO_2 particles accelerate the photodamage of skin due to their photocatalytic degradation activity. To effectively eradicate this unwanted effect, we present a new strategy toward the preparation of organic/inorganic hybrid polymer/TiO_2 nanoparticles with highly effective UV-screening property but eliminated photocatalytic activity. We prepared new polymer micelles with corona−shell−core structure based on self-assembly of poly(ethylene oxide)-*block*-poly(2-(dimethylamino)ethyl methacrylate)-*block*-poly(styrene) (PEO-*b*-PDMA-*b*-PS) triblock copolymer. Selective deposition of hydrophobic tetrabutyl titanate (TBT) in the PDMA shell in polar solvent leads to a thin PDMA/TiO_2 hybrid layer (~8 nm), which can not only effectively reflect UV rays but also eliminate its photocatalytic ability to protect skin. The sol−gel reactions of TBTs in the PS core domain lead to a PS/TiO_2 hybrid core, which can also absorb/reflect UV lights by PS/TiO_2. The biocompatible PEO coronas can prevent direct contact of TiO_2 with skin. Moreover, sol−gel reactions in the PDMA and PS domains can stabilize the triblock copolymer micelles, which offer the promising potential for further formulations in aqueous solution. The ATRP kinetics confirmed that PEO-*b*-PDMA-*b*-PS triblock copolymer can be synthesized in one pot, which simplified the synthetic procedure of copolymers. TEM and DLS studies revealed the morphology and size of self-assembled polymer micelles and the subsequent polymer/TiO_2 hybrid nanoparticles upon sol−gel reactions. UV experiments confirmed the highly efficient UV screening activity but eliminated photocatalytic property of polymer/TiO_2 hybrid nanoparticles. For example, at extremely low TiO_2 content in solution (10 ppm of polymer/TiO_2 solid), ~70% UV radiation can be blocked compared to pure organic polymer micelle, which is also much more efficient than commercially available TiO_2 nanoparticles (P25). UV and DLS studies confirmed the ultrahigh stability of polymer/TiO_2 hybrid nanoparticles upon strong UV radiation, which is suitable for long-term applications. Nitrogen adsorption/desorption experiment revealed that the ultralow surface area of TiO_2 nanoparticles (1.6 m^2 g^{-1}) is consistent with their extremely poor photocatalytic performance.

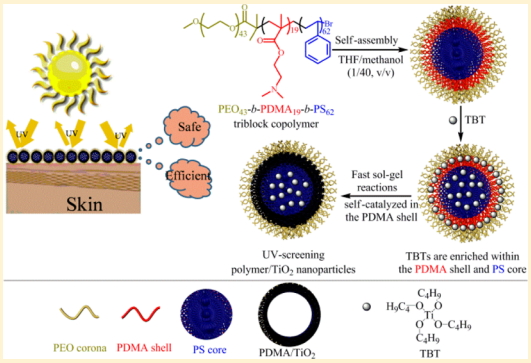

1. INTRODUCTION

Recently, increasing reports of skin cancer have made people increasingly aware of the danger of prolonged exposure to UV rays.[1] These account for about 6% of the terrestrial sunlight and have been proven to cause many diseases such as erythema, keratitis, cataracts, and certain skin cancers under excessive doses.[2] It is well-known that both organic and inorganic UV blockers have been developed to shield against UV radiation.[3,4] However, to achieve the designated sun protection factor (SPF) in sunscreen formulations, more inorganic nanoparticles are used to reflect/scatter the UV light, rather than using more organic molecules or particulates to absorb UV radiation. Inorganic titanium dioxide (TiO_2) is a low cost and highly stable semiconductor oxide,[5,6] which has been used as solar cells,[7−11] and noted to be a safe physical sunscreen (US Federal Register, 43FR38206) because it reflects and scatters UVB (290−320 nm) and UVA (320−400 nm) in sunlight.[12] However, inorganic TiO_2 nanoparticles have recently shown ineffective in sunscreen materials because they are accompanied by photocatalytic degradation activity, which in turn accelerates the photodamage of skin.[12] Fox example, inorganic TiO_2 nanoparticles can release reactive oxygen species, which have the capability to alter DNA.[13] Therefore, it is important to eradicate this unwanted photocatalytic activity of TiO_2 nanoparticles. In practice, either polymeric or inorganic thin layer was coated on the surface of TiO_2 nanoparticles to form a core−shell particle during the sunscreen formulation. Typical polymers include poly(hydroxystearic acid) and its alternatives. Recently, an antioxidant-grafted poly[methyl vinyl ether/maleic acid] layer was coated on TiO_2 nanoparticles by sonochemistry to block photocatalytic degradation ability by blocking the emission of surface electrons.[14] Usually, the inorganic coating layer is composed of silica (SiO_2) and alumina (Al_2O_3).[15] The above methods involved the coating of either polymeric or

Received: October 22, 2012
Revised: December 26, 2012
Published: January 9, 2013

 © 2013 American Chemical Society

Scheme 1. Strategy towards Highly Effective UV-Screening Polymer/TiO_2 Hybrid Nanoparticles with Eliminated Unwanted Photocatalytic Activity by Selectively Depositing TiO_2 in the Middle Shell and the PS Core of a Triblock Copolymer Micelle[a]

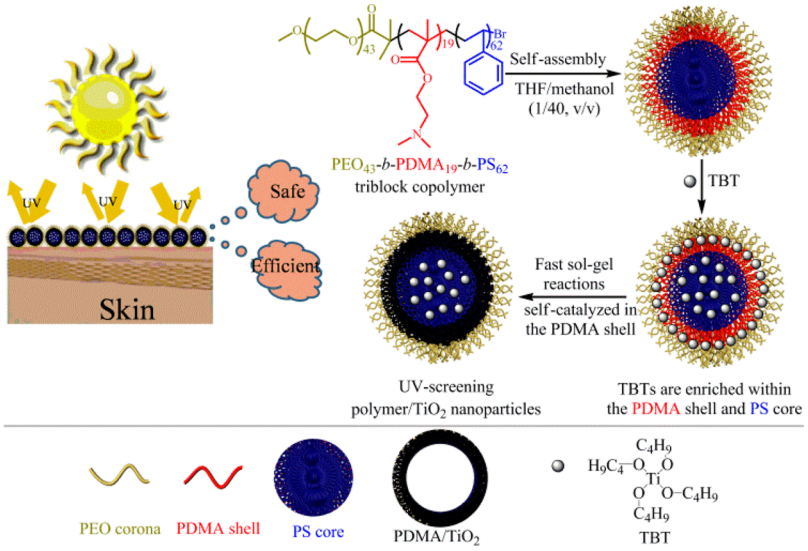

[a]First, the PEO_{43}-*b*-$PDMA_{19}$-*b*-PS_{62} copolymer self-assembles into polymer micelles. Second, the hydrophobic tetrabutyl titanates (TBTs) are enriched within the hydrophobic PDMA shell and PS core. Third, fast sol−gel reactions self-catalyzed by the PDMA shell lead to a PDMA/TiO_2 hybrid layer covered on the hydrophobic PS core, where subsequent slower sol−gel reactions lead to polymer/TiO_2 hybrid nanoparticles. Here, TiO_2 is the inorganic UV screening agent. The biocompatible PEO coronas can stabilize the hybrid nanoparticles and prevent TiO_2 from directly contacting skin. The PDMA can not only catalyze the sol−gel reactions but also block the emission of surface electrons in the PDMA/TiO_2 layer to decrease the photocatalytic activity of TiO_2. The PS core can support the polymer/TiO_2 hybrid nanoparticle and absorb UV radiation.

inorganic layer on the TiO_2 surface. Sometimes it is costly and troublesome to coat these ingredients. On the contrary, the selective deposition of TiO_2 into a multifunctional triblock copolymer micelle template represents an alternative strategy toward low cost and facile preparation of TiO_2 nanoparticles for highly effective UV-screening but eliminated photocatalytic activity.

It is well-known that amphiphilic copolymers can self-assemble into a range of nanostructures such as micelles[16−20] and vesicles,[21−24] which have shown increasingly diverse applications in material science. For example, polymer micelles have been used as drug delivery carrier,[25] sterilization agent,[19,26] in the preparation of calcite crystals,[27] and in templating silica growth.[28,29] Recently, poly(ethylene oxide)-*block*-polystyrene (PEO-*b*-PS) diblock copolymers are used for the incorporation of TiO_2 nanoparticles in the hydrophilic PEO domain due to hydrogen-bonding interactions between the PEO and −Ti-$(OH)_x$ (x = 1−4) groups on the surface of TiO_2 nanoparticles.[30−35] Other hydrophilic block such as poly(acrylic acid) (PAA) has been employed to introduce TiO_2 nanoparticles into the PAA core domain of diblock copolymer reverse micelles in toluene.[36] Also, TiO_2 nanoparticles have been selectively introduced into the PAA shell of a PS-*b*-PAA-*b*-PEO triblock copolymer micelle to afford hollow titania nanospheres upon calcinations, exhibiting excellent electrochemical properties in lithium ion rechargeable batteries.[37] Also, mesoporous titania coatings can be prepared using PEO-*block*-polybutadiene-*block*-PEO template.[38] Other polymer-based titania hybrid nanoparticles have also been reported via electrostatic interaction based adsorption[39,40] and covalent cross-linking.[41] However, to the best of our knowledge, neither the *in situ* generation of TiO_2 nanoparticles in the hydrophobic core of polymer micelles has been reported nor those hybrid nanoparticles have been explored as UV-screening product.

Herein, we prepare a new multifunctional polymer micelle based on the self-assembly of PEO-*b*-PDMA-*b*-PS triblock copolymer and then explore a new strategy for polymer/TiO_2 hybrid nanoparticles as the highly effective UV-screening agents with eliminated photocatalytic activity. As shown in Scheme 1, potential advantages of using polymer/TiO_2 hybrid nanoparticles as UV-screening agents are (i) selective deposition of hydrophobic tetrabutyl titanate (TBT) in the hydrophobic poly[2-(dimethylamino)ethyl methacrylate)] (PDMA) shell leads to a thin PDMA/TiO_2 hybrid layer (∼8 nm), which can effectively reflect UV rays and eliminate its photocatalytic ability to protect skin; (ii) sol−gel reactions in the PS domain leads to a PS/TiO_2 hybrid core, which can absorb/reflect UV lights; (iii) sol−gel reactions stabilize copolymer micelles, which offers the potential for further formulations in aqueous solution; and (iv) biocompatible PEO coronas prevent direct contact of TiO_2 with skin.

The polymer/TiO_2 hybrid nanoparticles are prepared in three steps: First, PEO_{43}-*b*-$PDMA_{19}$-*b*-PS_{62} triblock copolymer was synthesized by atom transfer radical polymerization (ATRP) according to the synthetic route in Scheme 2. Second, the copolymer self-assembles into micelles in methanol/THF. Third, the hydrophobic tetrabutyl titanate (TBT) is added into the copolymer micelle solution in methanol, which can be enriched in the hydrophobic PS core and PDMA shell to form polymer/TiO_2 hybrid nanoparticles by PDMA-catalyzed *in situ* sol−gel reactions. The rate of the sol−gel reactions in the PDMA shell is much faster than that in the PS core,[42,43] leading to a PDMA/TiO_2 hybrid layer surrounding the PS core. Polymer/TiO_2 hybrid nanoparticles were spontaneously formed upon further sol−gel reactions of TBT molecules confined in the PS core.

dx.doi.org/10.1021/ma3022019 | *Macromolecules* 2013, 46, 375−383

Scheme 2. Synthetic Route to the PEO_{43}-*b*-$PDMA_{19}$-*b*-PS_{62} Triblock Copolymer by ATRP

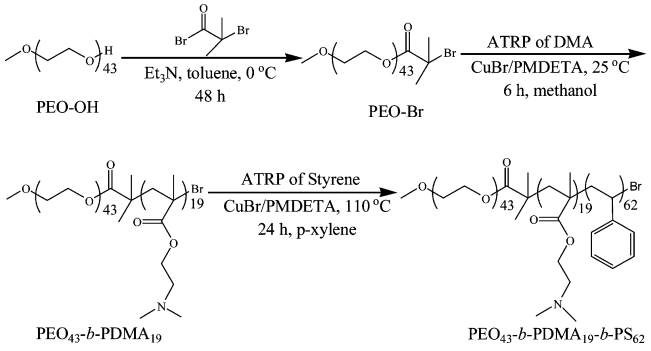

2. RESULTS AND DISCUSSION

2.1. Synthesis of PEO_{43}-*b*-$PDMA_{19}$-*b*-PS_{62} Triblock Copolymer. The synthetic route is shown in Scheme 2. First, PEO_{43}−Br macroinitiator was synthesized by esterification of poly(ethylene oxide) methyl ether with 2-bromoisobutyryl in toluene. The ^{1}H NMR spectrum in Figure 1a confirmed

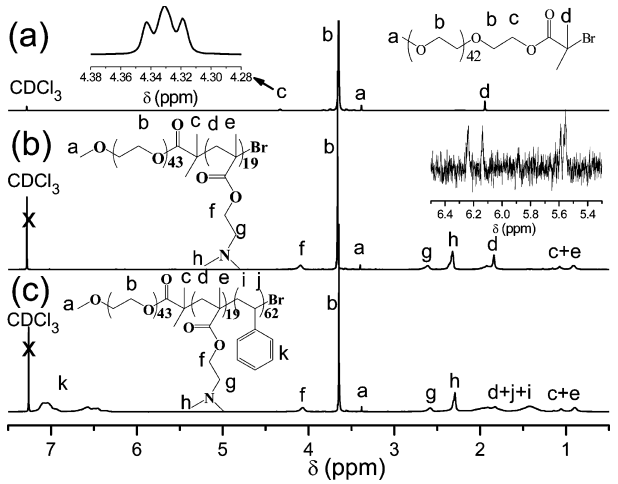

Figure 1. ^{1}H NMR spectra in $CDCl_3$: (a) PEO_{43}−Br macroinitiator, (b) PEO_{43}-*b*-$PDMA_{19}$ diblock copolymer without purification (except removing the methanol), and (c) PEO_{43}-*b*-$PDMA_{19}$-*b*-PS_{62} triblock copolymer. The magnified spectrum in (b) shows little residual DMA monomer.

~99% of esterification efficiency by comparing the integrated areas of peaks b and d, indicating the successful synthesis of the macroinitiator. DMF GPC gave an M_n of 1457 and M_w/M_n of 1.12. Second, the triblock copolymer was synthesized by sequent ATRP of DMA and styrene monomers by a one-pot approach to afford PEO_{43}-*b*-$PDMA_{19}$-*b*-PS_{62} triblock copolymer. In order to verify the successful synthesis of the PEO-*b*-PDMA-*b*-PS triblock copolymer rather than a *block-statistical* PEO-*b*-PDMA-*b*-P(DMA-*stat*-St) copolymer, we carried out the kinetic study on the DMA polymerization, as shown in Figure 3. An induction period was observed, indicating that some time was needed to establish a dynamic equilibrium between the Cu^I and partial oxidative Cu^{II} species at the earlier stage of polymerization,[44] while pseudo-first-order kinetics and linear growth of conversion rates were observed, which indicated the propagating radical concentration kept constant in the preceding time of polymerization.[45,46] The monomer conversion increases with the reaction time and reaches 80% within 2 h. The molecular weight determined by GPC increases with the monomer conversion and the polydispersity remains over a range of 1.2−1.3. After 6 h reaction, the monomer conversion has been >99% by comparing the integrated areas of peak b (−OCH_2CH−), peak h (−$N(CH_3)_2$), and peaks between δ 5.4−6.4 [CH_2=$C(CH_3)$−] from unreacted DMA monomer, as judged by ^{1}H NMR analysis of PEO_{43}-*b*-$PDMA_{19}$-Br diblock copolymer without purification (Figure 1b). These results confirmed the successful synthesis of PEO_{43}-*b*-$PDMA_{19}$ diblock copolymer and no residual DMA monomer. After 6 h, styrene and *p*-xylene were added to synthesize the PEO_{43}-*b*-$PDMA_{19}$-*b*-PS_{62} triblock copolymer.

The mean block composition of PEO_{43}-*b*-$PDMA_{19}$-*b*-PS_{62} was determined by comparing the integrated areas of peaks b (PEO), f, h (PDMA), and k (PS) in the ^{1}H NMR spectrum in Figure 1c. Both the ^{1}H NMR spectrum (Figure S1 in Supporting Information) and GPC data (M_n = 25 000, M_w/M_n = 1.37 by THF GPC; see Figure 2) confirmed the successful synthesis of PEO_{43}-*b*-$PDMA_{19}$-*b*-PS_{62} triblock copolymer.

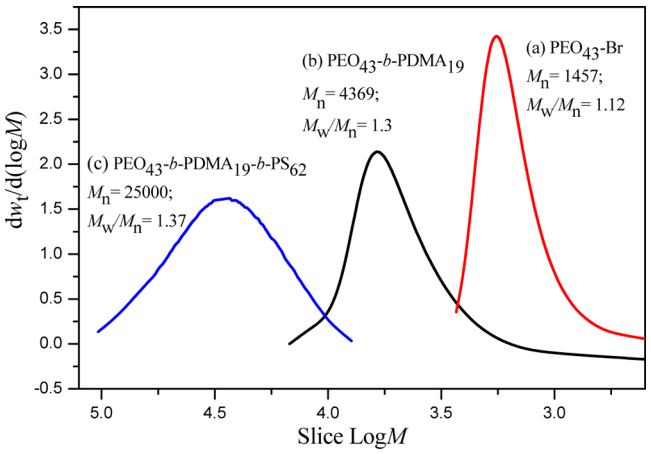

Figure 2. GPC traces of (a) PEO_{43}−Br macroinitiator, (b) PEO_{43}-*b*-$PDMA_{19}$-Br diblock copolymer eluted by DMF, and (c) PEO_{43}-*b*-$PDMA_{19}$-*b*-PS_{62} triblock copolymer eluted by THF.

2.2. Self-Assembly of Triblock Copolymer into Micelles. Well-defined polymer micelles were formed spontaneously when methanol was added into a solution of triblock copolymer in THF at room temperature (V_{MeOH}:V_{THF} = 40:1). PEO and PDMA are soluble while PS is insoluble in methanol. Thus, the PEO chains form the coronas and the PDMA chains form the shell, while the insoluble PS chains form the core of the micelles. Dynamic light scattering (DLS) studies indicate an intensity-averaged hydrodynamic diameter (D_h) of 140 nm with a low polydispersity (PD) of 0.112 (sample 1 in Table 1 and curve a in Figure 4). The corresponding volume- and number-averaged diameters are 123 and 88 nm, respectively (see Table 1 for details).

2.3. Polymer/TiO_2 Hybrid Nanoparticles. To prepare the polymer/TiO_2 hybrid nanoparticles, hydrophobic TBT was added into the copolymer micelle solution in methanol, which was then enriched in PDMA and PS domains in polar solution. The confined sol−gel reactions can afford polymer/TiO_2 hybrid nanoparticles. Different preparation conditions have been summarized in Table 1. DLS studies (samples 2 and 4 in Table 1) revealed that the D_h's were 147 and 145 nm by intensity (89 and 93 nm by number) with a low PD when the

dx.doi.org/10.1021/ma3022019 | Macromolecules 2013, 46, 375−383

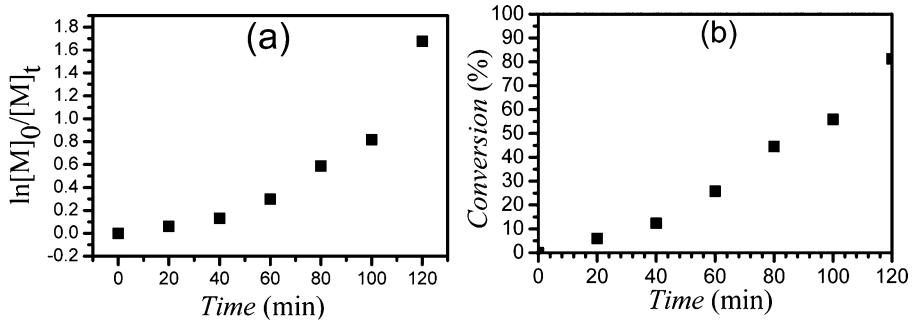

Figure 3. (a) Kinetic plots for the ATRP of DMA using PEO_{43}–Br as the macroinitiator in methanol at 25 °C. (b) Plots of DMA monomer conversion vs reaction time. Conditions: $[PEO\text{-}Br]_0/[CuBr]_0/[PMDETA]_0/[DMA]_0 = 1/1/1/19$.

Table 1. Summary of Preparation Conditions and DLS Studies of Polymer/TiO_2 Hybrid Nanoparticles

sample	DMA/TBT[a]	$D_{h,intensity}$[b] (nm)	$D_{h,volume}$[b] (nm)	$D_{h,number}$[b] (nm)	PD
1	1/0	140	123	88	0.112
2	1/0.4	147	126	89	0.135
3	1/0.6	149	133	91	0.132
4	1/0.8	145	129	93	0.108
5	1/1.0	218	147	73	0.351

[a]Molar ratio of DMA unit to tetrabutyl titanate (TBT). [b]Hydrodynamic diameters of polymer/TiO_2 hybrid nanoparticles by DLS by intensity, volume, and number, respectively. The initial concentration of polymer micelles before the addition of TBT is 0.5 mg/mL in THF/methanol (1/40, v/v), and the reaction time is 24 h..

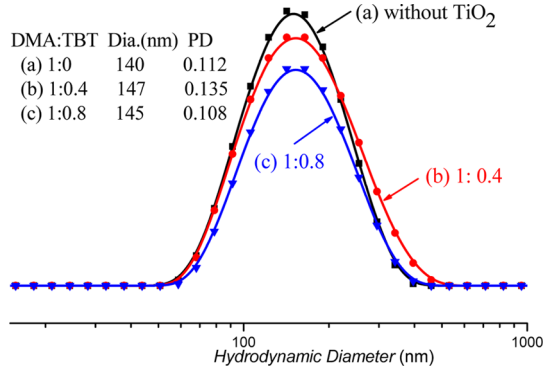

Figure 4. Intensity-averaged size distribution of PEO_{43}-*b*-$PDMA_{19}$-*b*-PS_{62} triblock copolymer micelles at 0.5 mg/mL by DLS before (a) and after (b, c) tetrabutyl titanate (TBT) deposition to form polymer/TiO_2 hybrid nanoparticles. The molar ratios of the DMA unit to the TBT are (a) 1:0 (without TiO_2), (b) 1:0.4, and (c) 1:0.8.

molar ratios of DMA:TBT were 1:0.4 and 1:0.8, respectively. Compared with the D_h of polymer micelles without TiO_2 (sample 1 in Table 1), the addition of TBT did not destroy the initial structure of the copolymer micelles. In addition, to test their water dispersibility, the polymer/TiO_2 hybrid nanoparticles (DMA:TBT is 1:0.4) were redispersed in water. DLS studies revealed that the intensity- and number-averaged diameters were 102 and 76 nm, respectively, with a very low PD of 0.063 at pH 6.7 (Figure 5), which are in good agreement with the sizes before TBT deposition. This excellent water dispersibility of the hybrid nanoparticle is very suitable for the formulation of UV-screening product. Moreover, this experiment confirms that there is little free TBT in the continuous

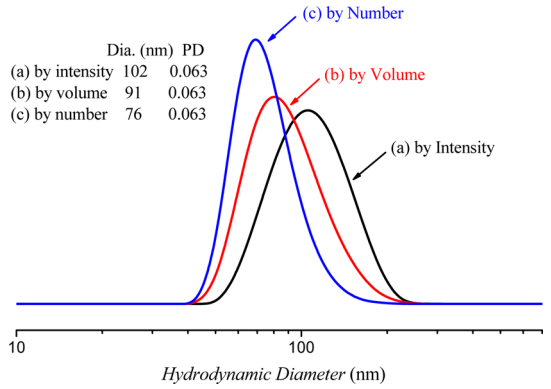

Figure 5. Particle size distribution of polymer/TiO_2 hybrid nanoparticles (TBT-deposited micelles) upon redispersion from THF/methanol to pure water at pH 6.7.

phase in methanol. Otherwise, the immediate macroscopic precipitation would be observed in the solution.

Besides the hydrophobic effect, the hydrogen bonding between TBT and PDMA is another reason for the selective deposition of TiO_2 in the PDMA shell. It is noteworthy that partially hydrolyzed TBT (due to trace of water in solvent) interacts with PDMA shell as a result of hydrogen bonding, which serves as both a scaffold and a catalytic template.[47,48] The rate of sol–gel reactions of TBT to TiO_2 is faster in the PDMA shell than that in PS core because of the self-catalysis of PDMA, as confirmed by the TEM images with a relatively darker ring in Figure 6A, according to a similar mechanism for the silica deposition in the PDMA coronas of PDMA–PDPA diblock copolymer micelles.[28] The faster sol–gel reactions led to a thin PDMA/TiO_2 hybrid layer on the PS core, which made the unreacted TBT molecules confined in the hydrophobic PS core, and in turn became titania upon further sol–gel reactions or calcinations. The number-averaged diameter of the polymer/TiO_2 hybrid nanoparticles in the TEM image is 71 ± 11 nm (Figure 6A), which is in good agreement with the diameter by DLS (76 nm by number in water at pH 6.7; see Figure 5) as the TEM only shows the PS core covered by the PDMA/TiO_2 hybrid layer (~8 nm thickness).

Usually, TBT can be hydrolyzed very quickly in polar solvents such as water and methanol to form macroscopic precipitates, which is not beneficial for the preparation of ordered nanostructures. However, sol–gel reactions in a confined domain may significantly decrease the reaction rate. Because TBT molecules can be selectively enriched in the PDMA shell and PS core of PEO_{43}-*b*-$PDMA_{19}$-*b*-PS_{62} triblock copolymer micelles, we think they may be able to effectively

dx.doi.org/10.1021/ma3022019 | Macromolecules 2013, 46, 375–383

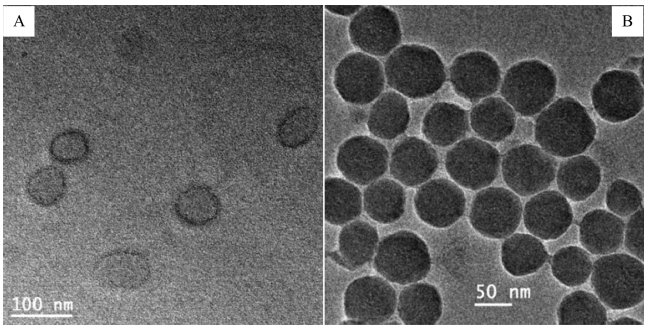

Figure 6. TEM images: (A) Polymer/TiO_2 hybrid nanoparticles before calcinations (DMA/TBT is 1:0.4, n/n). The thin dark layer (~8 nm) is PDMA/TiO_2 hybrid structure, which covers the PS core and is more electron-dense than the PS core. Please note that the particles have a solid rather than a hollow structure.[28] (B) TiO_2 nanoparticles after calcinations. The formation of the solid structure in (B) is a strong evidence of the successful loading of the hydrophobic TBTs into the hydrophobic PS micelle core. Otherwise, a hollow structure will appear after calcinations. A slower rate of sol–gel reactions in the PS core at ambient conditions is also confirmed by this figure due to the poor accessibility of the loaded TBTs to the water and the PDMA catalyst.

prevent the TBTs in methanol from ultrafast hydrolysis and polycondensation reactions.[42] This was confirmed by DLS results where the D_h's as a function of reaction time were recorded, as shown in Figure S2 of the Supporting Information. Both the particle size and PD demonstrated reasonable fluctuations. However, the white precipitation was immediately formed when the TBT was added into the pure methanol without polymer micelles, indicating fast sol–gel reactions.

Moreover, TEM images in Figure 6A do confirm that after 24 h sol–gel reactions, the TBTs in the PS domain did not form TiO_2. In contrast, the encapsulated TBTs were converted into well-defined solid TiO_2 nanoparticles upon calcinations (Figure 6B). If there are no TBTs in the PS domain, there would be a hollow structure after calcinations. Therefore, the TEM studies further confirmed a fast sol–gel rate of the TBTs in the PDMA shell and a slower sol–gel rate of the TBTs in the PS core at ambient conditions.

2.4. TiO_2 Nanoparticles. In a further control experiment, PS homopolymer was found to be soluble in TBT. Thus, when added to a methanol solution, the hydrophobic TBTs could be enriched within the hydrophobic PS core. To test this hypothesis and to prepare TiO_2 nanoparticles, the polymer/TiO_2 hybrid nanoparticles (TBT-deposited polymer micelles) were calcined at 800 °C. TGA curve revealed ~13% of residual solid (Figure S3). As shown in Figure 6B, TEM study confirmed the formation of TiO_2 nanoparticles after calcinations. The number-averaged diameter in the TEM image is 64 ± 12 nm, slightly less than that before calcinations (71 ± 11 nm). After calcinations, the diameter of nanoparticles decreased by 10% based on the TEM images, as a result of the shrinkage of the particle during the calcinations. It is noteworthy that this is different from the previously reported results that preformed TiO_2 only incorporated into the *hydrophilic PEO coronas* and usually hollow TiO_2 nanospheres were formed upon calcinations.[30−32,37] The formation of the solid TiO_2 spheres after calcinations is a strong evidence of the loading of the hydrophobic TBTs into the hydrophobic PS micelle core; otherwise, a hollow structure will appear after calcinations.

To reveal the surface area and the porosity of TiO_2 nanoparticles, the nitrogen adsorption/desorption measurement was carried out by Brunauer–Emmett–Teller (BET), as shown in Figure 7. The isotherm is classified as type IV and

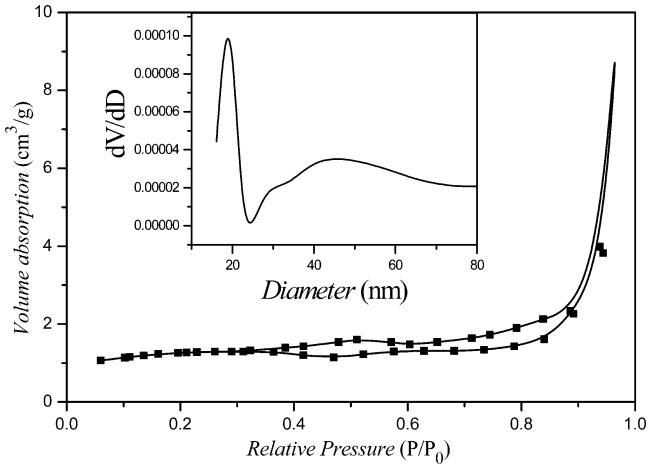

Figure 7. Nitrogen adsorption/desorption isotherm and corresponding pore size distribution curves of TiO_2 nanoparticles.

displays type H3 hysteresis loop (IUPAC 13.2). The plots of the pore size distributions are determined by the Barrett–Joyner–Halenda (BJH) method from the desorption branch of the isotherm, indicating the presence of mesoporous structure with an average diameter of 20 nm. However, the TEM image in Figure 6B did not reveal the corresponding pores. This discrepancy may be related to the theories in measuring the pore sizes. By BET, as various methods for the calculation of the pore size are based on the shape of the pores, sometimes the reliability of the pore size calculation is questionable. For example, the BJH method is based on the cylindrical and the slit-shaped assumption, which may be not the real pore shape. The specific surface area of our TiO_2 nanoparticles is only 1.6 $m^2\ g^{-1}$ by BET. Nevertheless, the very low surface area suggests the poor photocatalytic activity of the TiO_2 nanoparticles. Also, XRD confirmed the rutile phase of TiO_2 nanoparticles (Figure 8).

2.5. Comparison of Zeta Potentials among Pure Copolymer Micelles, Polymer/TiO_2 Hybrid Nanoparticles, and TiO_2 Nanoparticles. In water, the zeta potential

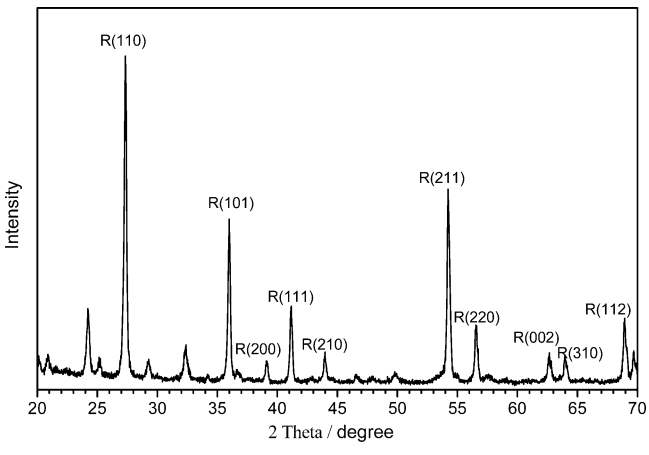

Figure 8. XRD pattern of rutile TiO_2 nanoparticles.

dx.doi.org/10.1021/ma3022019 | *Macromolecules* 2013, 46, 375–383

of the triblock copolymer micelles, polymer/TiO_2 hybrid nanoparticles (DMA:TBT = 1:0.4, n/n), and calcined TiO_2 nanoparticles, are +29.9, +23.5, and −18.1 mV, respectively. The positive charge (+29.9 mV) confirms the polymer micelles having PEO-*b*-PDMA corona−shell structure. The zeta potential of polymer/TiO_2 hybrid nanoparticles was slightly decreased to +23.5 mV as a result of the electrostatic interaction between the negatively charged TiO_2 nanoparticles and the positively charged PDMA shell. Also, it confirms the confined sol−gel reactions in the PDMA shell and the PS core, rather than in the hydrophilic PEO coronas. Otherwise, a negative zeta potential would be expected due to the surface-coated TiO_2. Actually, a negative charge (−18.1 mV) of TiO_2 nanoparticles is revealed as a result of calcinations where the organic composition is burned off.

2.6. UV-Screening Property of Organic/Inorganic Hybrid Nanoparticles. To test the UV-screening property of the polymer/TiO_2 hybrid nanoparticles, UV transmittance was measured at highly dilute solution of 0.01 mg/mL (~10 ppm), as shown in Figure 9 and Figure S4. The UV-

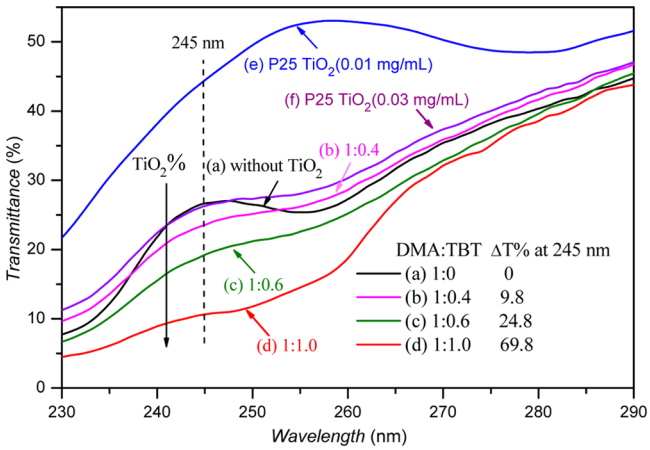

Figure 9. UV transmittance spectra of polymer/TiO_2 hybrid nanoparticles (a−d) and commercially available P25 TiO_2 at 0.01 mg/mL (~10 ppm, e) and 0.03 mg/mL (f) in methanol. The molar ratios of the DMA unit to TBT are (a) 1:0 (without TBT), (b) 1:0.4, (c) 1:0.6, and (d) 1:1.

transmittance ability at 237−253 nm wavelengths increases with the feeding TBT, which is consistent with the excellent UVC (200−280 nm)-shielding property of TiO_2.[49,50] At 245 nm, the ability to transmit UV rays decreases by 10%, 25%, and 70% when the DMA to TBT ratios are 1:0.4, 1:0.6, and 1:1, respectively, compared with polymer micelles without TBT deposition, indicating their excellent UV-screening property of polymer/TiO_2 hybrid nanoparticles. Comparing curves a and b, slight incorporation of TiO_2 reduces the ability to block UV rays at >254 nm wavelengths, possibly as a result of suppressive activity of benzene groups in PS/TiO_2 hybrid nanoparticles. Also, at the same concentration (0.01 mg/mL), the transmittance at 245 nm for the commercially available pure P25 TiO_2 nanoparticles is ~45% (curve e). In contrast, for the pure polymer micelles (curve a) a decreased percentage of ~25% and for polymer/TiO_2 hybrids a further decreased percentage of only ~9% (curve d) were observed, which confirmed the excellent UV-screening activities of polymer/TiO_2 hybrids.

However, the amount of scattering may correlate with the total amount of particles in the solution. Therefore, we tested the transmittance of UV irradiation in the presence of a higher concentration of P25 TiO_2 nanoparticles (0.03 mg/mL). As expected, the transmittance of UV irradiation at the whole wavelengths decreased (see curve f in Figure 9). The transmittance at 245 nm decreased from 44.6% to 19.2% when the concentration of P25 TiO_2 nanoparticles was increased from 0.01 to 0.03 mg/mL.

Here the question is that due to the different densities between P25 TiO_2 nanoparticles and the organic/inorganic hybrid nanoparticles, the amount of particles may be different at the same mass concentration, which eventually influences the transmittance of the solution. Therefore, we carried out the following further experiments. We found that the D_h of pure P25 TiO_2 nanoparticles is 76 nm (Figure S6), which is the same as our hybrid nanoparticles. The density of the commercially available P25 TiO_2 nanoparticles (130 kg/m^3) is lower than the hybrid nanoparticles (~692 kg/m^3), which means that at the same mass concentration much less amount of hybrid nanoparticles is presented in the solution than P25 TiO_2 nanoparticles. However, the hybrid nanoparticles perform much better during the UV-screening measurement than the commercially available P25 TiO_2 nanoparticles (comparing curves d and e).

2.7. Photocatalytic Property of Polymer/TiO_2 Hybrid Nanoparticles. The photocatalytic property of the polymer/TiO_2 hybrid nanoparticles was evaluated by measuring the decomposition rates of small molecules such as Rhodamine B in water. As shown in Figure 10, nearly 95% of Rhodamine B

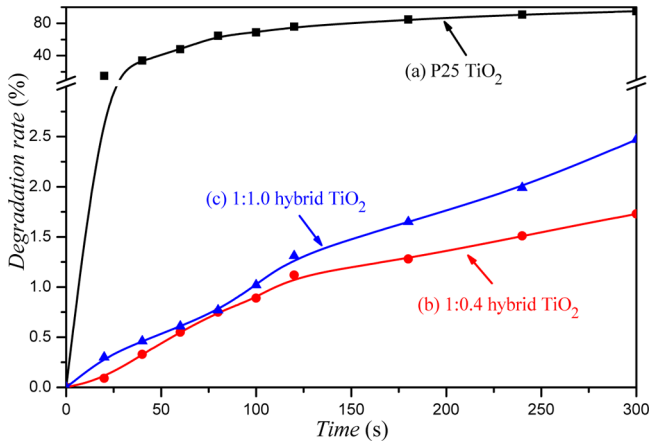

Figure 10. Plot of degradation rates of Rhodamine B (0.01 mg/mL) under strong UV radiation (8000 mW/cm^2) by (a) commercially available P25 TiO_2, (b) polymer/TiO_2 hybrid nanoparticles with the molar ratio of DMA to TBT of 1:0.4, and (c) polymer/TiO_2 hybrid nanoparticles with the molar ratio of DMA to TBT of 1:1.0 in H_2O (0.05 mg/mL).

(0.01 mg/mL) was degraded in 300 s in the presence of 0.05 mg/mL of commercially available P25 TiO_2 nanoparticles under strong UV radiation (8000 mW/cm^2), while only 2.5% of Rhodamine B was degraded in the presence of 0.05 mg/mL polymer/TiO_2 hybrid nanoparticles.

We also carried out the control experiments to evaluate the possible absorption of Rhodamine B by nanoparticles. Only 2% and no Rhodamine B were absorbed by P25 and polymer/TiO_2 hybrid nanoparticles in the absence of UV radiation (see Figure 11), respectively. These results indicated the excellent elimination of photocatalytic activity of polymer/TiO_2 hybrid

dx.doi.org/10.1021/ma3022019 | *Macromolecules* 2013, 46, 375−383

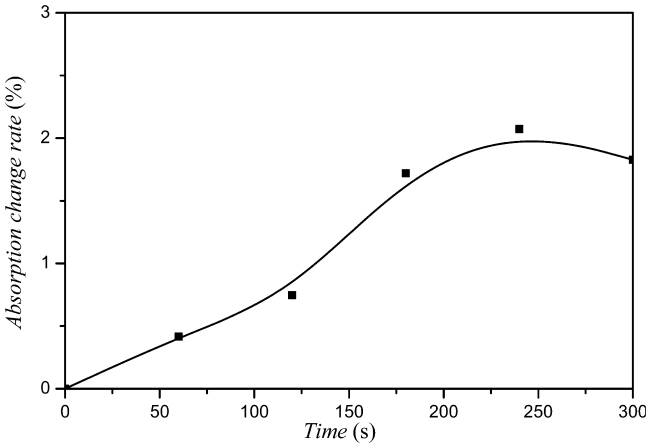

Figure 11. Plot of the variation in UV absorption of Rhodamine B (0.01 mg/mL) in darkness in the presence of P25 TiO_2 nanoparticles (0.05 mg/mL) in water. This experiment confirms the weak absorption of Rhodamine B by P25 TiO_2 nanoparticles. In contrast, no Rhodamine B was absorbed by polymer/TiO_2 hybrid nanoparticles (data not shown here).

nanoparticles, which may be used as new UV blockers without skin damage.

To investigate the possibility of self-degradation of polymers in the polymer/TiO_2 hybrid nanoparticles, their aqueous solution (0.05 mg/mL) was exposed to strong UV radiation (8000 mW/cm^2). By comparing the absorbance of benzene group at various radiation times, no obvious variations at the wavelength of ~265 nm were observed after 3 h, as shown in Figure 12. For example, after 1.5 and 3 h of UV radiation, the

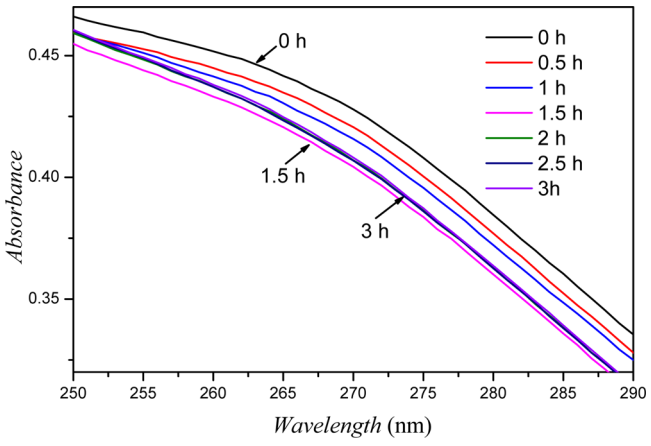

Figure 12. UV absorption spectra of polymer/TiO_2 hybrid nanoparticles under strong UV radiation at various exposure times. The concentration of the hybrid nanoparticles in H_2O is 0.05 mg/mL.

absorbance at 265 nm only decreased by 4.7% and 3.8%, respectively, indicating that the polymer micelle structure was not destroyed upon strong UV radiation. We did not observe any precipitation in the solution after long-time UV radiation, further suggesting the excellent stability of the polymer/TiO_2 hybrid nanoparticles. Moreover, DLS studies of the hybrid nanoparticles at different radiation times (see Figure 13) further confirmed the above explanation. For example, the hydrodynamic diameters of the polymer/TiO_2 hybrid nanoparticles kept at ~76 nm (by number) with low PD's. The corresponding diameters by intensity and volume were 110 and

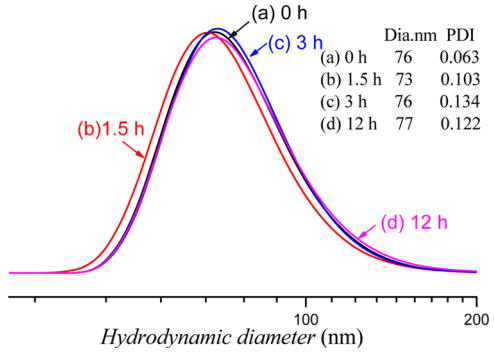

Figure 13. Size distributions of polymer/TiO_2 hybrid nanoparticles determined by DLS by number at 0.05 mg/mL and various UV radiation times: (a) 0, (b) 1.5, (c) 3, and (d) 12 h. The molar ratio of the DMA unit to TBT is 1:0.4.

90 nm, respectively (see Figure S5), indicating excellent stability of the hybrid nanoparticles in solution. The above results confirm the poor self-degradation of the hybrid nanoparticles under strong UV radiation, which is important for the formulation in aqueous media.

3. EXPERIMENTAL SECTION

3.1. Materials. Poly(ethylene oxide) methyl ether (MeO−PEO−OH; M_n ca. 1900; M_w/M_n = 1.10) was purchased from Alfa Aesar and dried azeotropically using anhydrous toluene to remove trace of water. 2-(Dimethylamino)ethyl methacrylate (DMA) was purchased from Sinopharm Chemical Reagent Co., Ltd., and passed through a silica gel column to remove the inhibitor. The P25 TiO_2 nanoparticles were kindly donated by Shanghai Haiyi Scientific & Trading Co., Ltd. 2-Bromoisobutyryl bromide, copper(I) bromide (CuBr, 99.999%), *N,N,N′,N″,N″*-pentamethyldiethylenetriamine (PMDETA, 98%), triethylamine, titanate precursor tetrabutyl titanate (TBT), Rhodamine B, *p*-xylene, tetrahydrofuran (THF), anhydrous ethanol, anhydrous methanol (>99%, Beijing Chemical Reagent Co.), and other reagents were purchased from Aladdin Chemistry Co. and used as received.

3.2. Characterization. DMF GPC: Gel permeation chromatography (GPC) analysis was carried out with a Waters Breeze 1525 GPC analysis system with two PL mix-D column, using DMF with 0.50 M LiBr as the eluent at a flow rate of 1.0 mL/min at 80 °C, PEO calibration kit (purchased from TOSOH) as the calibration standard.

THF GPC: GPC analysis was also carried out with a Waters 515 pump, a Waters 2414 refractive index detector, and a combination of Styragel HT-3 and HT-4. The effective molecular weight ranges were 100−10 000, 500−30 000, and 5000−60 000, respectively. The eluent was THF at a rate of 1.0 mL/min.

^{1}H NMR spectra were recorded using a Bruker AV 400 MHz spectrometer at ambient temperature using $CDCl_3$ as solvent.

Transmission electron microscopy (TEM) images were obtained using a JEM-2100 electron microscope equipped with a Gatan 1K × 1K digital camera operating at an acceleration voltage of 200 kV. To prepare TEM samples, 10 μL of diluted aqueous nanoparticle solution was placed on a copper grid coated with thin carbon film and dried under ambient conditions.

DLS and zeta potential studies were conducted at 25 °C using a Zetasizer Nano ZS90 instrument (Malvern Instruments) equipped with a multipurpose autotitrator (MPT-2) at a fixed scattering angle of 90°. The data were processed by Cumulants analysis of the experimental correlation function, and particle diameters were calculated from the computed diffusion coefficients using the Stokes−Einstein equation. Each reported measurement was conducted for three runs. For zeta potential studies, the polymer/TiO_2 hybrid nanoparticles and TiO_2 nanoparticles were dispersed in deionized water at pH 6.70 and pH 6.66, respectively.

UV−vis studies were conducted using a UV−vis spectrophotometer (Shanghai Precision & Scientific Instrument Co., Ltd., UV759S) with a

dx.doi.org/10.1021/ma3022019 | *Macromolecules* 2013, 46, 375−383

scan speed of 300 nm/min. The absorbance and transmittance spectra of the hybrid micelles in the range of 200−650 nm wavelengths were recorded. Degradation experiments under UV radiation were conducted using a Power Arc UV 100 light source at 8000 mW/cm^2.

Thermogravimetric analysis (TGA) experiments were conducted using a PerkinElmer thermal gravimetric and differential thermal analysis instrument (America) from room temperature to 1000 °C with a heating rate of 10 °C/min in air flow.

XRD studies were carried out using XRD (D/max 2550) with Cu Kα radiation at an angular domain between 20° and 70° (2θ).

Brunauer−Emmett−Teller (BET) experiment was carried out at −196 °C using a Micromeritics ASAP 2020 instrument. The pore size distribution was calculated from the desorption branch of the sorption isotherms using the Barret−Joyner−Halenda (BJH) method.

3.3. Synthesis of PEO_{43}−Br Macroinitiator. MeO−PEO−OH (10.00 g; 5.3 mmol) was dissolved in toluene (200 mL) in a 500 mL of flask in an oil bath at 130 °C, and a trace of water was removed by azeotropic distillation. Triethylamine (1.70 mL, 0.0132 mol) was added into the flask when the solution was cooled to room temperature. Then 2-bromoisobutyryl bromide (1.85 mL, 0.0132 mol) was dropped into the flask in 3 h. After 2 days, the insoluble salt was removed by filtration. After removal of toluene by rotary evaporation, the crude product was redissolved in dichloromethane and poured into water with vigorous stirring for 1 h. The organic phase was collected, and the water phase was extracted twice using dichloromethane. The combined organic solution was further washed with 1.0 M HCl and 1.0 M NaOH for three times successively. The combined organic phase was dried over anhydrous $MgSO_4$. Finally, the solution was concentrated and then precipitated in 500 mL of diethyl ether. The dissolution/precipitation cycle was repeated for three times. Yield: 80%.

3.4. Kinetic Studies of ATRP of DMA. In a Schlenk flask charged with a magnetic flea, PEO_{43}−Br macroinitiator (0.5000 g, 0.2469 mmol), PMDETA (0.0437 g, 0.2469 mmol), DMA (0.7922 g, 0.0049 mol), and methanol (3.0 mL) was added and deoxygenated with argon bubbles for 30 min. Then CuBr (0.0360 g, 0.2469 mmol) was added into the flask. The reaction was carried out at 25 °C under argon protection. In the first 2 h, 300 μL of the solution was withdrawn every 20 min. The reaction was stopped after 6 h to get PEO_{43}-*b*-$PDMA_{19}$ diblock copolymer. The monomer conversion was obtained by the gravimetric method, and the molecular weights of diblock copolymers were determined by GPC in DMF. The DMA monomer conversion after 6 h of reaction was >99% as judged by ^{1}H NMR.

3.5. Synthesis of PEO_{43}-*b*-$PDMA_{19}$-*b*-PS_{62} Triblock Copolymer by ATRP. In a Schlenk flask charged with a magnetic flea, PEO_{43}−Br macroinitiator (0.5000 g, 0.2469 mmol), PMDETA (0.0437 g, 0.2469 mmol), DMA (0.7922 g, 0.0049 mol), and methanol (2.0 mL) were added and deoxygenated with argon bubbles for 30 min. Then CuBr (0.0360 g, 0.2469 mmol) was added into the flask. The reaction was carried out at 25 °C under argon protection. Six hours later, deoxygenated styrene (1.818 g, 0.0173 mol) in *p*-xylene (3.0 mL) was added into the flask. The reaction was carried out at 110 °C for 16 h. Then the reaction solution was diluted in excess THF, passing through a silica column to remove the spent copper catalyst. The solution was concentrated and then precipitated in methanol. The product was dried in a vacuum oven at 25 °C overnight. Yield: 70%.

3.6. Self-Assembly of Triblock Copolymer. PEO_{43}-*b*-$PDMA_{19}$-*b*-PS_{62} triblock copolymer (20.0 mg) was dissolved in THF (1.0 mL). Methanol (40.0 mL) was added dropwise with vigorous stirring.

3.7. Deposition of TBT into Copolymer Micelles. The titanate precursor TBT (1.0 g) was first diluted in ethanol (10.0 g). In an ample with copolymer micelle solution (5.0 mL), TBT/ethanol with different molar ratios of DMA to TBT (see Table 1) was added under vigorous stirring for 24 h at room temperature. The initial concentration of polymer micelles before the addition of TBT was 0.5 mg/mL in THF/methanol (1/40, v/v).

3.8. Redispersion of Polymer Micelles or Polymer/TiO_2 Hybrid Nanoparticles into Water. The polymer micelles or polymer/TiO_2 hybrid nanoparticles solution (100 μL, 0.5 mg/mL) in THF/methanol (1/40, v/v) was poured into H_2O (1.0 mL) under vigorous stirring. The organic solvents were then removed by dialysis or rotary evaporator. The solution pH was adjusted by aqueous NaOH or HCl solution.

3.9. Calcinations of Polymer/TiO_2 Nanoparticles. The dried polymer/TiO_2 hybrid nanoparticles were calcined at 800 °C in a muffle for 3 h in air. The X-ray diffraction (XRD) pattern of TiO_2 nanoparticles in Figure 6B is shown in Figure 8. The sharp diffraction peaks strongly indicated exclusive rutile phase of TiO_2.[51] In particular, the diffraction peaks at 2θ = 27.3, 36.0, 39.1, 41.1, 44.0, 54.2, 56.6, 62.7, 64.0, and 69.0 are related to the (110), (101), (200), (111), (210), (211), (220), (002), (310), and (112) reticular planes of rutile.

3.10. Degradation of Rhodamine B by Polymer/TiO_2 Hybrid Nanoparticles under UV Radiation. Aqueous Rhodamine B solution (0.01 mg/mL) and dried polymer/TiO_2 hybrid nanoparticles were dispersed in deionized H_2O (0.05 mg/mL, 10 mL) in the aid of ultrasonic sound and illuminated using Power Arc UV 100 at 8000 mW/cm^2. The final pH of the solution is 6.7. The absorbance of Rhodamine B at 542 nm was calculated by subtracting the absorbance of pure polymer/TiO_2 hybrid nanoparticles without Rhodamine B in water under the same conditions as in the presence of Rhodamine B.

4. CONCLUSIONS

In summary, a new PEO-*b*-PDMA-*b*-PS triblock copolymer was synthesized by ATRP in one pot using PEO-Br as the macroinitiator. The ATRP kinetics confirmed that no residual DMA monomer before adding the second monomer, styrene. NMR and GPC confirmed the successful synthesis of triblock copolymer. The triblock copolymer was self-assembled into polymer micelles with PEO as the corona, PDMA as the shell, and PS as the core, which was confirmed by TEM and DLS studies. The micelles were subsequently used to mediate the formation of polymer/TiO_2 hybrid nanoparticles, as confirmed by TEM and DLS. Those hybrid nanoparticles exhibited highly effective UV-screening property but eliminated photocatalytic activity, as well as high stability upon strong UV radiation, as confirmed by a series of UV experiments and DLS studies. It is confirmed that the PDMA block is important because it serves as both scaffold and catalyst for the confined sol−gel reactions of TBTs in the PDMA shell and for in-situ blocking the emission of surface electrons in the PDMA/TiO_2 layer to minimize the photocatalytic activity. In addition, PEO coronas can protect skin and stabilize the polymer/TiO_2 hybrid nanoparticles in aqueous solution. Nitrogen adsorption/desorption experiment reveals extremely low surface area of nanoparticles, which is consistent with their eliminated photocatalytic activity. Overall, we have exploited a new strategy toward highly effective and safe UV-screening polymer/TiO_2 hybrid nanoparticles.

■ ASSOCIATED CONTENT

Ⓢ Supporting Information

Figures S1−S6 and Tables S1 and S2, showing ^{1}H NMR spectra, TGA curve, more DLS and UV data, etc. This material is available free of charge via the Internet at http://pubs.acs.org.

■ AUTHOR INFORMATION

Corresponding Author

*E-mail jzdu@tongji.edu.cn; Tel +86-21-6958-0239; Fax +86-21-6958-4723.

Notes

The authors declare no competing financial interest.

■ ACKNOWLEDGMENTS

J.D. is supported by Shanghai 1000 Plan (SH01068), the program for professor of special appointment (Eastern Scholar) at Shanghai Institutions of Higher Learning (P2009011), National Natural Science Foundation of China (21074095 and 21174107), New Century Excellent Talents in Universities of Ministry of Education (NCET-10-0627), Ph.D. program Foundation of Ministry of Education (20110072110048), Fok Ying Tong Education Foundation (132018), Pujiang project of Shanghai Science and Technology Commission (10PJ1409900), the fundamental research funds for the Central Universities, the Bayer Science & Education Foundation, Bayer-Tongji Eco-Construction & Material Academy (TB20120004), and the open fund for characterization (0002012025) of Tongji University. Prof. Rachel K. O'Reilly at Warwick University is thanked for useful discussions.

■ REFERENCES

(1) Habibi, M. H.; Nasr-Esfahani, M.; Emtiazi, G.; Hosseinkhani, B. *Curr. Nanosci.* **2010**, *6*, 324−329.
(2) Beasley, D. G.; Meyer, T. A. *Am. J. Clin. Dermatol.* **2010**, *11*, 413−421.
(3) Sundarrajan, S.; Chandrasekaran, A. R.; Ramakrishna, S. *J. Am. Ceram. Soc.* **2010**, *93*, 3955−3975.
(4) Montazer, M.; Pakdel, E.; Moghadam, M. B. *Fibers Polym.* **2010**, *11*, 967−975.
(5) Iskandar, F.; Nandiyanto, A. B. D.; Yun, K. M.; Hogan, C. J.; Okuyama, K.; Biswas, P. *Adv. Mater.* **2007**, *19*, 1408−1412.
(6) Fujishima, A.; Zhang, X. T.; Tryk, D. A. *Surf. Sci. Rep.* **2008**, *63*, 515−582.
(7) Jang, Y. J.; Kim, D. H. *Chem.—Eur. J.* **2011**, *17*, 540−545.
(8) Koo, H. J.; Kim, Y. J.; Lee, Y. H.; Lee, W. I.; Kim, K.; Park, N. G. *Adv. Mater.* **2008**, *20*, 195−199.
(9) Li, X. F.; Zhang, L. A.; Wang, Y. X.; Yang, X. L.; Zhao, N.; Zhang, X. L.; Xu, J. A. *J. Am. Chem. Soc.* **2011**, *133*, 3736−3739.
(10) Mao, S. S.; Chen, X. B.; Liu, L.; Yu, P. Y. *Science* **2011**, *331*, 746−750.
(11) Tachikawa, T.; Yamashita, S.; Majima, T. *J. Am. Chem. Soc.* **2011**, *133*, 7197−7204.
(12) Dunford, R.; Salinaro, A.; Cai, L. Z.; Serpone, N.; Horikoshi, S.; Hidaka, H.; Knowland, J. *FEBS Lett.* **1997**, *418*, 87−90.
(13) Tran, D. T.; Salmon, R. *Australas. J. Dermatol.* **2011**, *52*, 1−6.
(14) Lee, W. A.; Pernodet, N.; Li, B. Q.; Lin, C. H.; Hatchwell, E.; Rafailovich, M. H. *Chem. Commun.* **2007**, 4815−4817.
(15) Popov, A. P.; Zvyagin, A. V.; Lademann, J.; Roberts, M. S.; Sanchez, W.; Priezzhev, A. V.; Myllyla, R. *J. Biomed. Nanotechnol.* **2010**, *6*, 432−451.
(16) O'Reilly, R. K.; Hawker, C. J.; Wooley, K. L. *Chem. Soc. Rev.* **2006**, *35*, 1068−1083.
(17) Read, E. S.; Armes, S. P. *Chem. Commun.* **2007**, 3021−3035.
(18) Du, J. Z.; O'Reilly, R. K. *Chem. Soc. Rev.* **2011**, *40*, 2402−2416.
(19) Yuan, W. Z.; Wei, J. R.; Lu, H.; Fan, L.; Du, J. Z. *Chem. Commun.* **2012**, *48*, 6857−6859.
(20) Du, J. Z.; Chen, Y. M. *Macromol. Rapid Commun.* **2005**, *26*, 491−494.
(21) Du, J. Z.; Armes, S. P. *J. Am. Chem. Soc.* **2005**, *127*, 12800−12801.
(22) Chen, Y.; Du, J.; Xiong, M.; Guo, H.; Jinnai, H.; Kaneko, T. *Macromolecules* **2007**, *40*, 4389−4392.
(23) Zhang, C.; Zhu, Y. Q.; Zhou, C. C.; Yuan, W. Z.; Du, J. Z. *Polym. Chem.* **2013**, *4*, 255−259.
(24) Du, J. Z.; Fan, L.; Liu, Q. M. *Macromolecules* **2012**, *45*, 8275−8283.
(25) Yoshida, M.; Lahann, J. *ACS Nano* **2008**, *2*, 1101−1107.
(26) Lu, H.; Fan, L.; Liu, Q. M.; Wei, J. R.; Ren, T. B.; Du, J. Z. *Polym. Chem.* **2012**, *3*, 2217−2227.
(27) Kim, Y.-Y.; Ganesan, K.; Yang, P.; Kulak, A. N.; Borukhin, S.; Pechook, S.; Ribeiro, L.; Kröger, R.; Eichhorn, S. J.; Armes, S. P.; Pokroy, B.; Meldrum, F. C. *Nat. Mater.* **2011**, *10*, 890−896.
(28) Yuan, J. J.; Mykhaylyk, O. O.; Ryan, A. J.; Armes, S. P. *J. Am. Chem. Soc.* **2007**, *129*, 1717−1723.
(29) Du, J. Z.; Armes, S. P. *Soft Matter* **2010**, *6*, 4851−4857.
(30) Gutierrez, J.; Tercjak, A.; Mondragon, I. *J. Am. Chem. Soc.* **2010**, *132*, 873−878.
(31) Scalarone, D.; Tata, J.; Caldera, F.; Lazzari, M.; Chiantore, O. *Mater. Chem. Phys.* **2011**, *128*, 166−171.
(32) Gutierrez, J.; Tercjak, A.; Garcia, I.; Peponi, L.; Mondragon, I. *Nanotechnology* **2008**, *19*, 155607.
(33) Zhang, J. Y.; Deng, Y. H.; Gu, D.; Wang, S. T.; She, L.; Che, R. C.; Wang, Z. S.; Tu, B.; Xie, S. H.; Zhao, D. Y. *Adv. Energy Mater.* **2011**, *1*, 241−248.
(34) Cheng, Y. J.; Gutmann, J. S. *J. Am. Chem. Soc.* **2006**, *128*, 4658−4674.
(35) Zhang, Y.; Tan, H.; Li, H.; Liu, Y.-Q.; Kartawidjaja, F. C.; Yang, Z.-C.; Wang, J. *Chem. Mater.* **2011**, *23*, 2745−2752.
(36) Yamada, S.; Mouri, E.; Yoshinaga, K. *J. Polym. Sci., Polym. Chem.* **2011**, *49*, 712−718.
(37) Sasidharan, M.; Nakashima, K.; Gunawardhana, N.; Yokoi, T.; Inoue, M.; Yusa, S.-i.; Yoshio, M.; Tatsumi, T. *Chem. Commun.* **2011**, *47*, 6921−6923.
(38) Ortel, E.; Fischer, A.; Chuenchom, L.; Polte, J.; Emmerling, F.; Smarsly, B.; Kraehnert, R. *Small* **2012**, *8*, 298−309.
(39) Hong, J.; Kang, S. W. *Ind. Eng. Chem. Res.* **2010**, *49*, 9124−9127.
(40) Song, L. X.; Lam, Y. M.; Boothroyd, C.; Teo, P. W. *Nanotechnology* **2007**, *18*, 135605.
(41) Siebert, M.; Albrecht, K.; Spiertz, R.; Keul, H.; Moller, M. *Soft Matter* **2011**, *7*, 587−594.
(42) Du, J. Z.; Armes, S. P. *Langmuir* **2008**, *24*, 13710−13716.
(43) Du, J. Z.; Armes, S. P. *Langmuir* **2009**, *25*, 9564−9570.
(44) Zhang, L. F.; Miao, J.; Cheng, Z. P.; Zhu, X. L. *Macromol. Rapid Commun.* **2010**, *31*, 275−280.
(45) Davis, K. A.; Matyjaszewski, K. *Macromolecules* **2001**, *34*, 2101−2107.
(46) Matyjaszewski, K.; Xia, J. H. *Chem. Rev.* **2001**, *101*, 2921−2990.
(47) Chen, T.; Colver, P. J.; Bon, S. A. F. *Adv. Mater.* **2007**, *19*, 2286−2289.
(48) Teng, G. H.; Wegner, J. R.; Hurtt, G. J.; Soucek, M. D. *Prog. Org. Coat.* **2001**, *42*, 29−37.
(49) Jiang, X.; Tian, X. Z.; Gu, J.; Huang, D.; Yang, Y. Q. *Appl. Surf. Sci.* **2011**, *257*, 8451−8456.
(50) Asahi, R.; Morikawa, T.; Ohwaki, T.; Aoki, K.; Taga, Y. *Science* **2001**, *293*, 269−271.
(51) Ye, J.; Liu, W.; Cai, J.; Chen, S.; Zhao, X.; Zhou, H.; Qi, L. *J. Am. Chem. Soc.* **2011**, *133*, 933−940.